ACCSCIENCE PUBLISHING

Explora: Environment and Resource

ORIGINAL RESEARCH ARTICLE

A novel one-step simulation–optimization framework for multi-crop actual evapotranspiration estimation

Halil Karahan*

Department of Civil Engineering, Faculty of Engineering, Pamukkale University, Denizli, Türkiye

Abstract

Accurate estimation of actual evapotranspiration (ETa) is essential for sustainable water management and irrigation planning. This study presents a simulation–optimization framework, integrated with the Simple Algorithm for Evapotranspiration Retrieving (SAFER) model, for daily ETa estimation and applies it to a heterogeneous agricultural region with multiple crop types. Unlike conventional SAFER implementations that rely on linear regression or trial-and-error calibration, the proposed framework enables simultaneous calibration of model coefficients via a single optimization procedure while preserving the model's nonlinear structure. Daily ETa was estimated using remote sensing inputs, including normalized difference vegetation ındex, land surface temperature (LST), surface albedo (αs), and meteorological data. The model was evaluated under two different training–testing scenarios to assess its robustness and generalization capability. Scenario I, which used only 38 satellite overpass days for calibration, achieved a test R^2 of 0.8195 and an overall R^2 of 0.8152. These results were consistent with Scenario II (test R^2 = 0.8249; overall R^2 = 0.8181), indicating stable predictive performance across different data partitioning schemes. The optimized coefficients remained highly consistent across scenarios ($a \approx 0.315$, $b \approx -0.0012$), demonstrating stable parameter convergence and robustness of the optimization process. Overall, the results indicate that reliable ETa estimation can be achieved even with limited calibration data, highlighting the practical applicability of the proposed framework for water management in data-scarce regions.

Keywords: Actual evapotranspiration; Simulation–optimization; Metaheuristic optimization; Remote sensing; Water resources management; Crop-based analysis

***Corresponding author:**
Halil Karahan
(hkarahan@pau.edu.tr)

Citation: Karahan H. A novel one-step simulation–optimization framework for multi-crop actual evapotranspiration estimation. *A Explora Environ Resour.* 2026;3(3):026210019. doi: 10.36922/EER026210019

Received: May 18, 2026

Revised: June 24, 2026

Accepted: June 29, 2026

Published online: July 15, 2026

Copyright: © 2026 Author(s). This is an Open-Access article distributed under the terms of the Creative Commons Attribution License, permitting distribution, and reproduction in any medium, provided the original work is properly cited.

Publisher's Note: AccScience Publishing remains neutral with regard to jurisdictional claims in published maps and institutional affiliations.

1. Introduction

Estimating actual evapotranspiration (ETa) is critical for effective water resource management and agricultural irrigation planning. Accurate ETa estimation plays a key role in characterizing the hydrological cycle and improving agricultural water use efficiency.

In recent years, several energy balance-based approaches have been developed to estimate crop water consumption using remote sensing data. Among the most widely used models are the surface energy balance algorithm for land[1], mapping evapotranspiration at high resolution with ınternalized calibration[2], and simplified surface energy balance.[3]

In addition to these approaches, Teixeira[4] proposed the Simple Algorithm for Evapotranspiration Retrieving (SAFER), a computationally efficient and biophysically consistent method designed primarily for irrigated areas in semi-arid regions. SAFER estimates the ETa fraction (ETf = ETa/ETo) using remote sensing variables such as the normalized difference vegetation ındex (NDVI), spectral reflectance data, land surface temperature, and basic meteorological inputs. By integrating vegetation status and surface energy balance components with reference ETa (ETo) derived from the Penman–Monteith method, SAFER enables reliable spatial estimation of ETa.[5–9]

The Penman–Monteith equation[10] is widely accepted as the standard method for estimating ETo. However, its practical application is often constrained by high data requirements, which have motivated the development of simplified alternative approaches. One such method is the Hargreaves–Samani equation[11], which requires only maximum and minimum air temperature data. Although SAFER-based studies predominantly rely on Penman–Monteith-derived ETo[7,12], applications using simplified ETo formulations remain limited.[6]

Given its physical basis and data efficiency, SAFER's performance can be further improved through local calibration of its parameters, particularly when applied across heterogeneous agricultural landscapes. The implementation of SAFER typically requires Landsat 8 imagery, including visible and near-infrared bands (B2–B5), shortwave infrared bands (B6–B7), and thermal infrared bands (B10–B11). These spectral inputs are used to derive key biophysical variables, including surface albedo, brightness temperature, land surface temperature (LST), and NDVI.[13]

Several studies have demonstrated the successful application of SAFER for estimating ETa at daily and monthly scales. Representative examples include Nadeem *et al.*[14], Nascimento Leão *et al.*[15], and Venancio *et al.*[16], all of which emphasize the necessity of parameter recalibration and the challenges associated with transferring calibrated coefficients across different climatic and cropping conditions.[17,18]

To address these limitations, Karahan *et al.*[19] proposed an artificial neural network (ANN)–based model for daily ETa estimation using limited meteorological and remote sensing inputs, including NDVI and LST. Their approach integrated satellite overpass data without temporal interpolation and demonstrated strong predictive performance (R^2 = 0.84), highlighting the potential of data-efficient modeling strategies.

In this study, a simulation–optimization (S/O) framework based on heuristic optimization techniques is proposed for calibrating SAFER model parameters. Daily ETa is estimated using NDVI, LST, surface albedo (αs), and available meteorological data, consistent with the input structure used in Karahan *et al.*[19] To evaluate model robustness under different data availability conditions, two scenarios are considered: Scenario I, which uses a limited training dataset, and Scenario II, which combines satellite overpass observations with long-term measurements.

The results demonstrate strong agreement between observed and predicted ETa values across both scenarios, confirming the robustness, stability, and practical applicability of the proposed S/O–SAFER framework for large-scale, multi-crop ETa estimation.

2. Materials and methods

2.1. Study area and data used

The study area is located in the Lower Seyhan, in the southeastern part of the Mediterranean Region of Türkiye (Figure 1). It is located approximately 30 km from Adana's city center and covers an area of 9,495 hectares. The Lower Seyhan Plain is a typical deltaic plain characterized by very flat topography, with slopes generally less than 1%, and an extensive irrigation and drainage network.[19,20]

Agricultural activity in the region is intensive, with two cropping seasons per year (summer and winter). The dominant crop types include citrus and various rotational crops that reflect the diversified agricultural structure of the area.[21]

Meteorological data used in this study were obtained from the L8 and Çotlu meteorological stations located within the study area.[19,21] The dataset includes daily observations of minimum and maximum air temperature (Tmin, Tmax), wind speed (U), solar radiation (Rs), minimum and maximum relative humidity (RHmin, RHmax), and precipitation (P). In total, the dataset consists of 769 consecutive daily records covering the period from September 16, 2020, to October 24, 2022.[19]

Reference ETa (mm/day) was calculated using the FAO-56 Penman–Monteith method[10], which is widely recognized as the standard approach for ETo estimation (**Equation 1**).

$$\mathrm{ETo} = \frac{0.408\Delta\,(\mathrm{R_n} - \mathrm{G}) + \gamma \frac{900}{\mathrm{T}+273}\mathrm{u}_2\,(\mathrm{e_s} - \mathrm{e_a})}{\Delta + \gamma\,(1 + 0.34\mathrm{u}_2)} \quad (1)$$

where Eto (mm/day) represents the rate of ETa from a reference surface; net radiation (Rn; MJ/m²/day) denotes the balance between incoming and outgoing radiation; soil heat flux (G; MJ/m²/day) represents the heat transfer

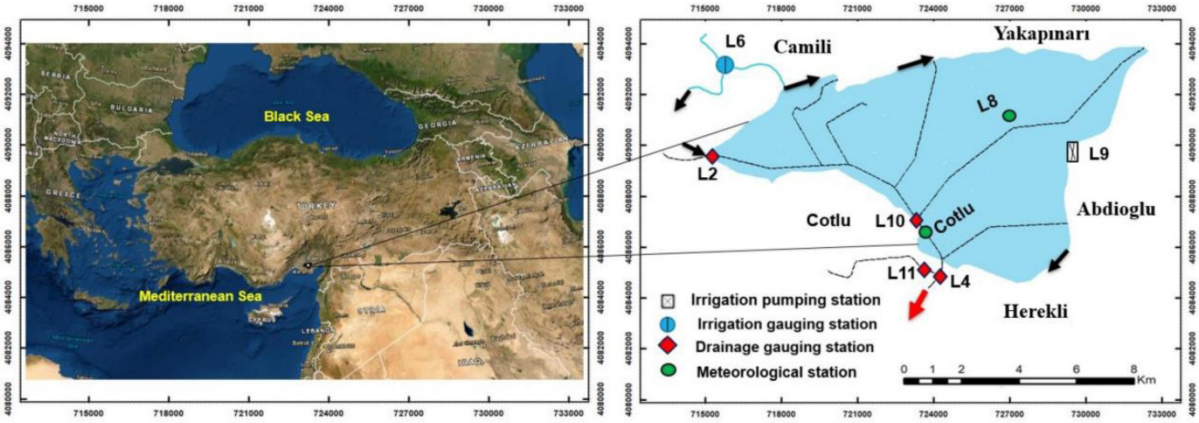


Figure 1. The study area is located in the southeastern Mediterranean region of Türkiye

into the soil; (es − ea) is the vapor pressure deficit (kPa); γ is the psychrometric constant (kPa/°C); Δ denotes the slope of the saturation vapor pressure–temperature curve (kPa/°C); u_2 (m/s) is the wind speed measured at 2 m above the ground surface; and T (°C) is the mean air temperature, calculated as the average of daily minimum and maximum temperatures.

Satellite data required for actual ETa estimation and for mapping high-resolution evapotranspiration using an internalized calibration model were obtained from the United States Geological Survey (USGS) EarthExplorer platform (http://earthexplorer.usgs.gov).[2,22]

In addition, the NDVI and LST products derived from the MODIS dataset were obtained via the Google Earth Engine platform[23–25] and harmonized with those used by Karahan *et al.*[19] The use of an identical dataset structure ensures direct comparability between the proposed model and the ANN-based approach presented in Karahan *et al.*[19]

To evaluate the linear relationships between independent variables (LST, albedo, NDVI, Rs, ETo) and the dependent variable (ETa), a Pearson correlation coefficient matrix was constructed, and the results are presented in Figure 2.

When the correlation matrix in Figure 2 and the descriptive statistics in Table 1 WERE jointly evaluated, the results indicate strong and physically consistent relationships among the variables. In general, ETa showed the strongest association with ETo and Rs, whereas its correlations with LST, albedo, and NDVI were comparatively weaker. This suggests that atmospheric demand and radiative forcing variables play a more dominant role in explaining ETa variability, while the remaining variables provide complementary information that supports model robustness rather than acting as primary drivers.

Table 1. Descriptive statistics of the dataset used in the study

Statistic	LST	Alpha	NDVI	ETo	ETa
Mean	28.066	0.154	0.505	3.476	3.070
Standard deviation	9.002	0.016	0.064	1.757	1.190
Min	7.050	0.116	0.340	0.466	0.612
Max	45.490	0.186	0.738	8.084	6.967
Median	31.690	0.154	0.501	3.416	3.099
Q1	19.773	0.143	0.459	1.800	2.165
Q3	35.370	0.165	0.550	5.026	3.922
Interquartile range	15.598	0.022	0.091	3.226	1.757
Skewness	−0.419	−0.192	0.295	0.139	0.068
Kurtosis	1.894	2.495	2.709	1.781	2.322

Abbreviations: Alpha: Surface albedo; ETa: Actual evapotranspiration; ETo: Reference evapotranspiration; LST: Land surface temperature; NDVI: Normalized difference vegetation index.

In particular, the very high correlation between ETo and ETa (r = 0.896) indicates that actual ETa is largely controlled by atmospheric water demand, suggesting an "atmospheric demand-driven" system behavior. Similarly, the strong relationship between LST and ETo (r = 0.854) demonstrates that surface temperature is a key regulator of evaporative demand, highlighting the dominant role of climatic forcing. The correlation between LST and ETa (r = 0.719), although weaker, indicates that this effect is primarily mediated by ETa through ETo.

The NDVI exhibited weak correlations with all variables ($r \approx 0.15$–0.30), indicating limited coupling with climatic drivers. This behavior can be attributed to land use

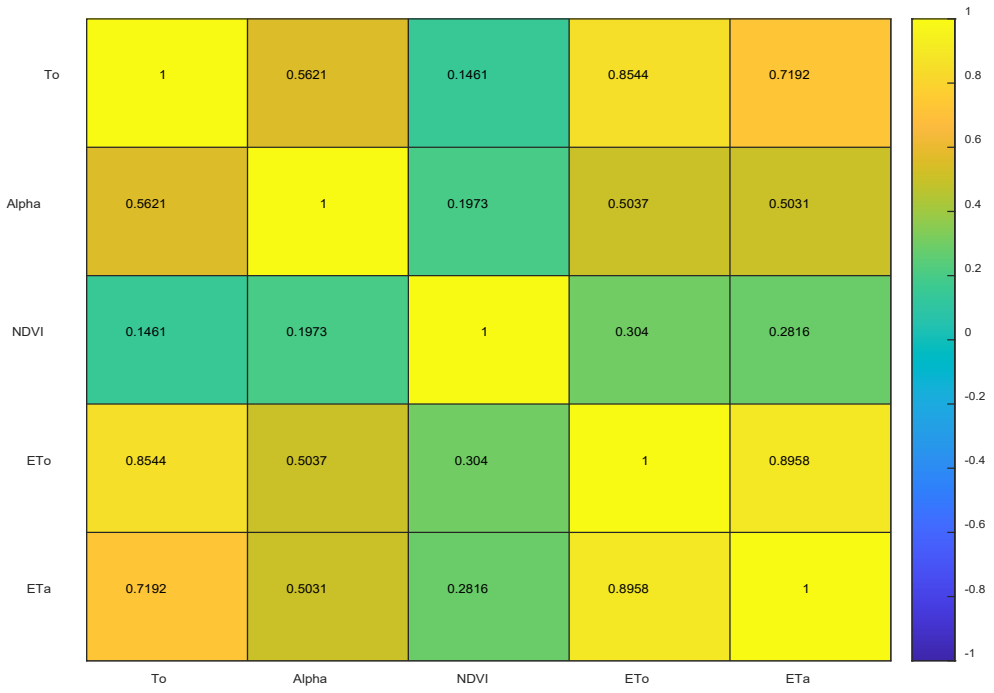


Figure 2. Correlation structure between ETa and model variables
Abbreviations: Alpha: Surface albedo; ETa: Actual evapotranspiration; ETo: Reference evapotranspiration; LST: Land surface temperature; NDVI: Normalized difference vegetation index.

characteristics of the study area, where approximately 45% consists of citrus orchards (perennial evergreen vegetation) and the remaining areas are under intensive agricultural practices with 2–3 cropping cycles per year. As a result, NDVI remains relatively stable throughout the year and should be interpreted not as a direct climatic indicator, but rather as an anthropogenically influenced phenological stability metric.

The alpha variable showed moderate correlations with LST, ETo, and ETa (≈0.50–0.56), indicating that surface properties are moderately linked to climatic processes, although their explanatory strength remains limited compared to the primary forcing variables.

When considered alongside the descriptive statistics in Table 1, the 769-day dataset represents short- to medium-term hydro-meteorological dynamics and exhibits structural signals consistent with long-range dependence frameworks discussed by Dimitriadis *et al.*[26] LST showed high variability, with a standard deviation of 9.00 and a wide range (7.05–45.49), while ETo exhibited similarly strong variability and extreme values, confirming its role as a key climatic forcing component. This structure suggests that both variables may exhibit persistent behavior (H > 0.5).

Actual evapotranspiration, characterized by more balanced statistical properties (standard deviation = 1.190, skewness ≈ 0.068), is a dependent response variable influenced jointly by atmospheric demand and surface conditions, exhibiting moderate-to-strong long-memory behavior. In contrast, NDVI showed low variability (standard deviation = 0.064) and a narrow range (0.340–0.738), reflecting a stable structure driven not by ecological limitation but by intensive agricultural activity and anthropogenic stabilization. Figure 3 illustrates the temporal variations of the variables used in the model, while Figure 4 presents the correlation relationships between the model variables and the observed ETa.

Overall, when both correlation patterns and statistical properties are considered, the system is consistent with a non-Markovian, scale-dependent, and partially persistent hydro-climatic structure in line with Dimitriadis *et al.*[26], where LST and ETo act as primary climatic drivers, while NDVI partially decouples from this long-memory structure due to land use–driven anthropogenic effects.

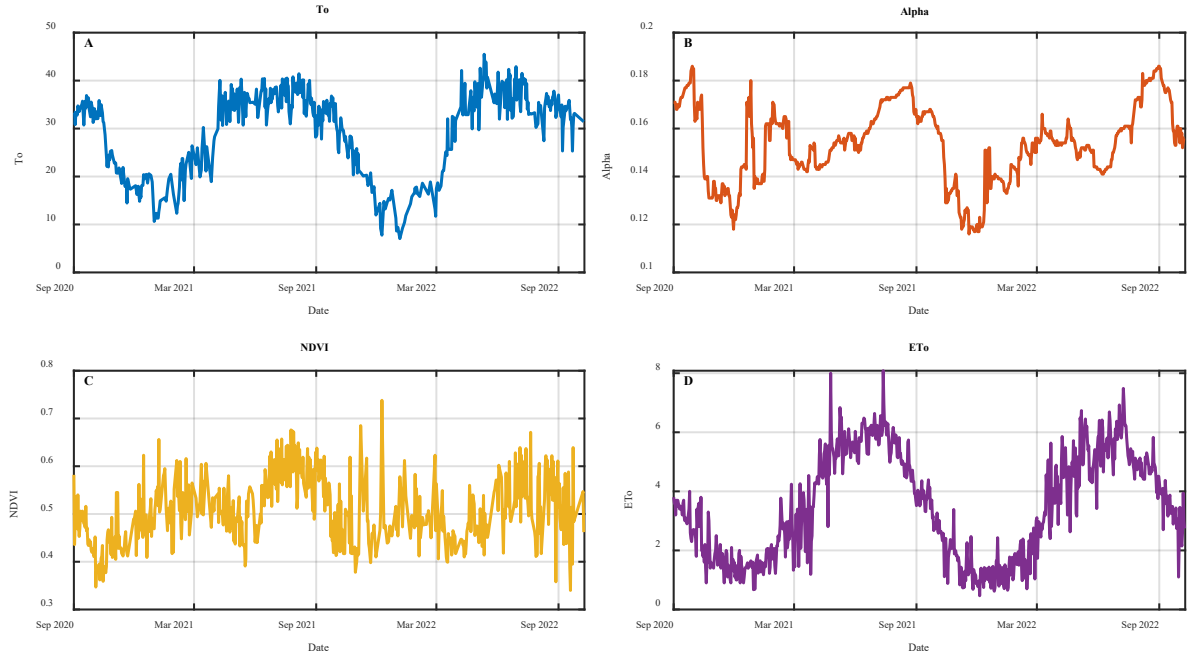


Figure 3. Temporal variation of the input variables used in the model. (A) LST. (B) Alpha. (C) NDVI. (D) ETo.
Abbreviations: Alpha: Surface albedo; ETo: Reference evapotranspiration; LST: Land surface temperature; NDVI: Normalized difference vegetation index.

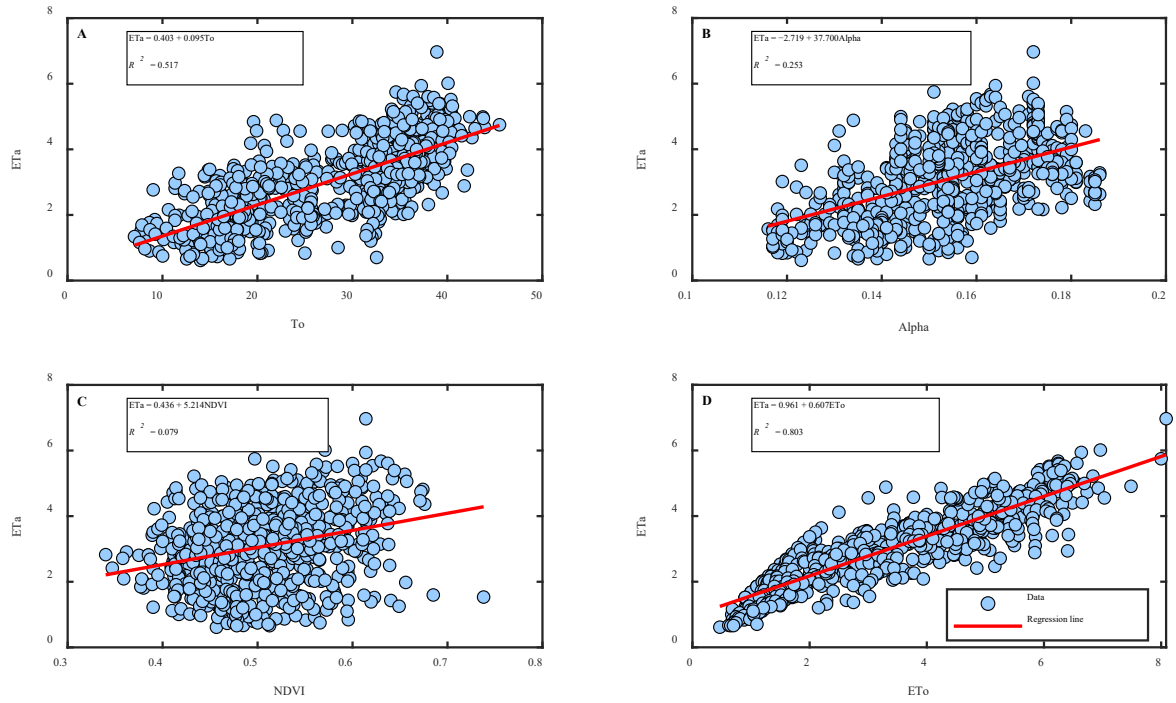


Figure 4. Correlation relationships between ETa and the model input variables. (A) LST. (B) Alpha. (C) NDVI. (D) ETo.
Abbreviations: Alpha: Surface albedo; ETa: Actual evapotranspiration; ETo: Reference evapotranspiration; LST: Land surface temperature; NDVI: Normalized difference vegetation index.

2.2. Simple Algorithm for Evapotranspiration Retrieving model

The SAFER model is an energy-balance-based approach used to estimate ETa by integrating physical parameters derived from satellite imagery with meteorological data from ground-based stations[4,8] The model is widely recognized for its simplicity of implementation, applicability under extreme environmental conditions, independence from detailed crop classification, and effective use of the ET/ETo ratio combined with remote sensing-derived variables.[27]

The SAFER model was originally developed and validated using field observations from irrigated agricultural areas and the caatinga ecosystem within the semi-arid Middle–Lower São Francisco River Basin. It has since been demonstrated to be an effective tool for ETa estimation, particularly in regions where *in situ* data availability is limited.[6] The model formulation is expressed as follows (**Equation 2**):

$$ET_a = \exp\left[a+b\left(\frac{T_0}{\alpha_s \cdot NDVI}\right)\right]ET_0 \quad (2)$$

where a and b are the empirical regression (calibration) coefficients, which are optimized based on site-specific conditions, satellite sensor characteristics, and climatic variability; T_0 is the land surface temperature derived from thermal infrared bands or equivalent thermal indicators; αs is the surface albedo at pixel level; NDVI is the normalized difference vegetation ındex representing vegetation density and vigor; Eta is the actual ETa (mm/day); and Eto is the reference ETa (mm/day).

In classical applications, the calibration parameters (a and b) are typically estimated using linear regression between concurrent satellite-derived variables and ground-based measurements such as eddy covariance flux tower data or lysimeter observations. This site-specific calibration step is essential for improving model accuracy and ensuring regional adaptability[7,18,28,29]

2.3. Simulation–optimization–Simple Algorithm for Evapotranspiration Retrieving and symbiotic organisms search algorithm

To enhance the predictive performance of the SAFER model, an S/O framework was adopted to calibrate the empirical coefficients a and b. Unlike classical calibration approaches such as linear regression, which estimate fixed parameters based on a single global relationship, the S/O framework enables adaptive parameter tuning under varying climatic and surface conditions. This improves the model's flexibility and generalization capability.

Within this framework, the symbiotic organisms search (SOS) algorithm was employed as the optimization engine. Proposed by Cheng and Prayogo[30], SOS is a population-based metaheuristic algorithm inspired by symbiotic interactions in natural ecosystems. Each candidate solution represents a potential parameter set (a, b), and solutions are iteratively improved through three interaction mechanisms:

(i) Mutualism phase: Two candidate solutions interact and both benefit by moving toward a shared advantageous region, typically guided by their average position and the current best solution.
(ii) Commensalism phase: One solution improves by exploiting the information from another solution without affecting it.
(iii) Parasitism phase: A solution modifies another to generate a new candidate; if the new solution has better fitness, it replaces the original.

These interaction strategies provide a balanced search mechanism by combining exploration (global search of the parameter space) and exploitation (refinement of promising regions), thereby increasing the probability of converging to a global optimum.

The SOS algorithm has been successfully applied in various hydrological and water resources optimization problems. For instance, when calibrating the nonlinear Muskingum flood routing model for the Karun River, SOS outperformed the genetic algorithm and harmony search, achieving lower error values.[31] Similarly, in reservoir operation studies such as those conducted for the Safarud Reservoir, SOS demonstrated fast convergence and high solution accuracy in identifying optimal operational policies.[32] These findings confirm the robustness and efficiency of SOS for nonlinear parameter estimation and water resources optimization problems.

The proposed S/O–SAFER optimization framework operates in three sequential phases:

(i) Initialization phase: Initial candidate solutions for parameters a and b are randomly generated within predefined search bounds.
(ii) Evaluation phase: For each candidate solution, ETa is computed using the SAFER model, and model performance is evaluated by comparing predicted and observed values using the mean squared error (MSE) as the objective function.
(iii) Optimization phase: The SOS algorithm iteratively updates candidate solutions by minimizing the objective function, progressively guiding the search toward an optimal parameter set while avoiding

entrapment in local minima.

Through this procedure, the SAFER model parameters are locally optimized in a data-driven manner, enabling more reliable ETa estimation across heterogeneous surface and climatic conditions.

2.4. Model evaluation and optimization framework

The S/O–SAFER model's performance was evaluated by comparing daily measured ETa values with model predictions. The statistical indicators used included[33]:

(i) MSE: Quantifies the magnitude of prediction errors (mm/day).
(ii) Mean absolute error (MAE): Represents the average absolute difference between predicted and observed values (mm/day).
(iii) Coefficient of determination (R^2): Measures the proportion of variance explained by the model.

During optimization, the SOS algorithm was used to determine the optimal a and b parameters by minimizing the MSE-based objective function. For all experiments, the SOS configuration was defined with a population size of NP = 50, and the search space boundaries for the parameters a and b were set to [−10, 10]. The optimization process was terminated when the maximum number of iterations was reached (or the convergence criterion was satisfied), ensuring computational consistency across all scenarios.

For each candidate parameter set generated by SOS, ETa values were computed using the SAFER model, and predictions were compared against observed measurements. The iterative optimization process was repeated until the stopping criterion was met, yielding the parameter set that minimizes the prediction error.

Results across various data scenarios and meteorological conditions indicate that the S/O-SAFER framework consistently achieves lower error metrics and higher correlation (R^2) values than the classical SAFER calibration approach.

The integration of satellite-derived variables (NDVI, surface temperature, and surface albedo) with ETo significantly enhances model accuracy and enables local adaptation to different crop types and surface conditions. Overall, the S/O–SAFER model demonstrates superior performance in both optimization efficiency and predictive accuracy compared to conventional calibration methods.

3. Results

3.1. Application of the Simple Algorithm for Evapotranspiration Retrieving model

The S/O–SAFER model generates daily ETa estimates by integrating key remote sensing and meteorological variables, including NDVI, LST, ETo, solar radiation (Rs), and MODIS-derived surface albedo (αs). As shown in Figure 3, the model parameters exhibit significant temporal variability, reflecting complex nonlinear dynamics that cannot be adequately captured by linear regression-based calibration approaches. This behavior highlights the need for a nonlinear S/O framework to properly capture parameter evolution and improve ETa estimation accuracy.

Traditional derivative-based nonlinear optimization techniques are often sensitive to initial parameter settings and constrained search domains, and they may converge to local minima rather than the global optimum.[34,35] To address these limitations, the SOS algorithm was employed. SOS provides a robust population-based search mechanism that balances exploration and exploitation in the solution space, enabling effective calibration of the nonlinear SAFER model parameters. In this study, SOS was used as the primary optimization engine; however, the framework remains flexible and can be extended to alternative metaheuristic optimization algorithms.

To evaluate the robustness and generalization capability of the proposed model, two different experimental scenarios were designed:

(i) Scenario I: 38 satellite overpass days were used for model training, while the remaining 731 days were reserved for testing.
(ii) Scenario II: 80% of the full 769-day dataset was randomly assigned for training, and the remaining 20% was used for testing.

3.1.1. Scenario I

In Scenario I, the model achieved R^2 values of 0.7294 and 0.8195 for the training and testing datasets, respectively. The corresponding root MSE (RMSE) values were 0.6910 (training) and 0.5694 (testing). When evaluated over the entire dataset, the model yielded an R^2 of 0.8152 and an RMSE of 0.5774. These results are consistent with the regression analysis presented in Figure 5.

The close alignment between the 1:1 reference line and the regression fit indicates strong agreement between observed and predicted ETa values. This suggests that the model accurately reproduces the underlying ETa dynamics

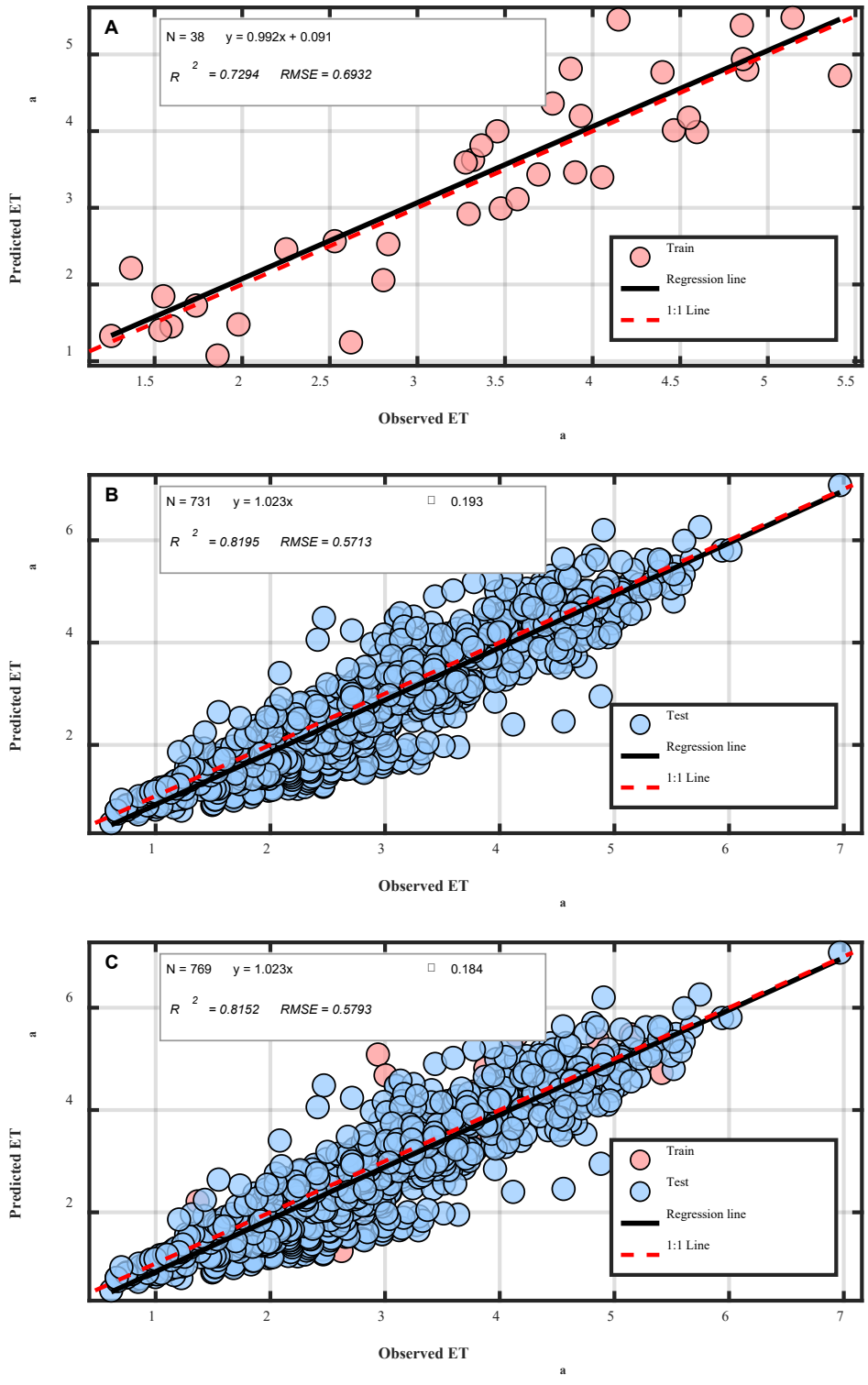


Figure 5. Comparison between observed and predicted ETa values for (A) training, (B) test, and (C) full datasets (Scenario I)

with minimal systematic bias.

As shown in Figure 6, the seasonal variation in model performance is minimal, highlighting the model's stability and high generalization capability across different temporal conditions.

3.1.2. Scenario II

In Scenario II, 80% of the dataset was used for model training, yielding optimized parameter values $a = 0.311686$ and $b = -0.001216$ obtained via the SOS-based calibration process. When evaluated on the complete dataset, the model achieved an R^2 of 0.8181 and an RMSE of 0.5584, as illustrated by the scatter plots in Figure 7.

The close agreement between the 1:1 reference line and the regression fit indicates a strong consistency between observed and predicted ETa values. This result further confirms the robustness of the proposed model under randomly partitioned training–testing conditions and highlights its generalization capability across the full dataset.

As depicted in Figure 8, the model maintains consistent performance across different seasons, suggesting that it effectively captures the underlying ETa dynamics rather than seasonal fluctuations. This further highlights its robustness and strong generalization capability under varying climatic conditions.

3.2. Comparison of simulation–optimization–Simple Algorithm for Evapotranspiration Retrieving model performance with alternative models

To assess the effectiveness of the proposed S/O–SAFER framework, its performance was compared with three widely used calibration and optimization approaches: LR, the Nelder–Mead simplex algorithm, and the Broyden–Fletcher–Goldfarb–Shanno (BFGS) algorithm.

Linear regression establishes a relationship between dependent and independent variables under the assumption of linearity.[36] Although computationally efficient and easy to interpret, it has limited ability to represent complex nonlinear relationships, potentially reducing predictive accuracy in heterogeneous agricultural environments.

The Nelder–Mead simplex algorithm is a derivative-free local optimization technique that iteratively updates a simplex to minimize an objective function.[37] While it can effectively handle nonlinear optimization problems without gradient information, its performance may be affected by the risk of converging to local minima.

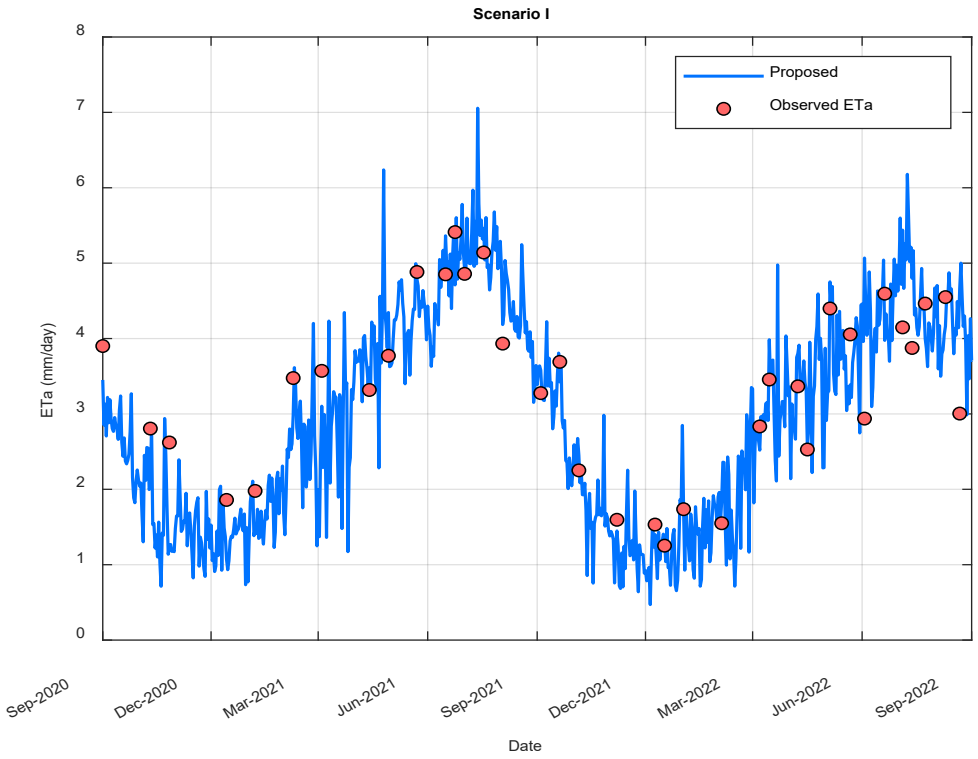


Figure 6. Temporal variation of model results for Scenario I, illustrating the seasonal stability and general agreement of predicted ETa with observations

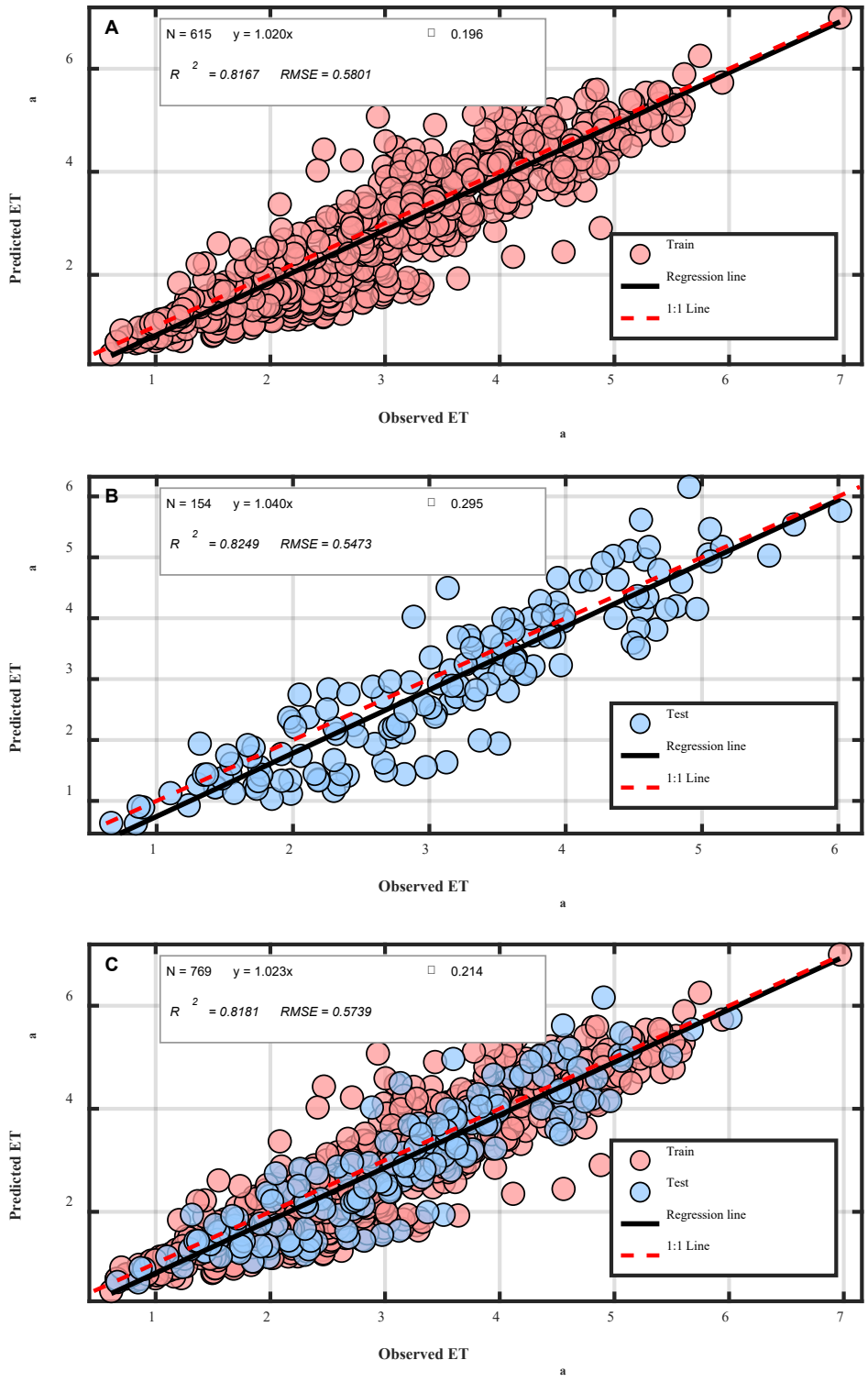


Figure 7. Model results for Scenario II, showing the comparison between observed and predicted ETa values for (A) training, (B) test, and (C) full datasets

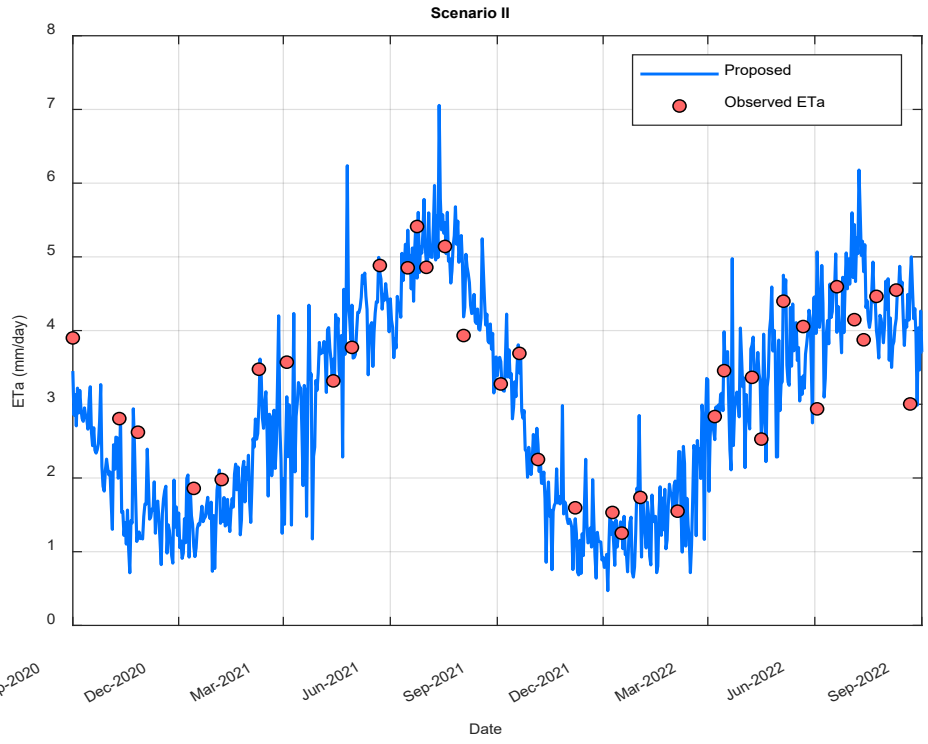


Figure 8. Temporal variation of model results for Scenario II, demonstrating the consistent alignment of predicted and observed ETa values throughout the study period

The BFGS algorithm is a quasi-Newton optimization method that approximates the Hessian matrix to efficiently locate the optimum of a smooth objective function.[38] Although generally faster than Nelder–Mead, its performance can be sensitive to the choice of initial parameter values and data quality.

3.2.1. Model calibration and performance metrics

The S/O–SAFER model estimates daily ETa using NDVI, LST, surface albedo (αs), and ETo. The model parameters were calibrated using the proposed SOS-based one-step S/O framework. To evaluate predictive performance, S/O–SAFER was benchmarked against linear regression, Nelder–Mead, and BFGS under two different calibration scenarios:

- Scenario I: Only the 38 satellite overpass days were used for calibration, while the remaining 731 days were reserved for model evaluation.
- Scenario II: The complete dataset (769 days) was randomly divided into 80% training and 20% testing subsets.

Model performance was evaluated using the MSE, MAE, RMSE, and R^2. The optimized parameter values (a and b) and the corresponding performance metrics for the training, testing, and full datasets are summarized in Table 2.

3.2.2. Comparative performance across scenarios

The comparative evaluation of the S/O–SAFER model against benchmark approaches—linear regression, Nelder–Mead, and BFGS optimization—demonstrates clear and consistent performance advantages across both Scenario I and Scenario II, as summarized in Table 2. The assessment is based on multiple statistical indicators, including MSE, MAE, RMSE, and R^2 across training, testing, and full datasets.

Overall, the S/O–SAFER model exhibited superior predictive accuracy and generalization capability in both scenarios. In Scenario I, which represents a more challenging setting with limited training data, the model achieved a testing R^2 of 0.8195 and an overall R^2 of 0.8152. These values indicate strong explanatory power despite data constraints. In Scenario II, performance improves slightly, with testing and overall R^2 values reaching 0.8249 and 0.8181, respectively, confirming the model's robustness and stability across different data configurations.

Table 2. Performance comparison of S/O–SAFER, linear regression, Nelder–Mead, and BFGS models under Scenarios I and II

Model	Scenario	Model parameters		Dataset	MSE	MAE	RMSE	R^2
		a	*b*					
S/O–SAFER	I	0.3148	−0.0012	Training	0.4848	0.5312	0.6962	0.7294
				Testing	0.3421	0.4548	0.5849	0.8195
				All data	0.3492	0.4586	0.5909	0.8152
	II	0.3158	−0.0012	Training	0.3604	0.4652	0.6003	0.8167
				Testing	0.3245	0.4479	0.5696	0.8249
				All data	0.3532	0.4617	0.5943	0.8181
Linear regression		0.4395	−0.0014	Training	0.3732	0.4778	0.6109	0.7342
				Testing	0.4184	0.5130	0.6468	0.7076
				All data	0.3868	0.4884	0.6219	0.7265
Nelder–Mead	I	0.2927	−0.0012	Training	0.3310	0.4440	0.5753	0.7643
				Testing	0.3919	0.4893	0.6260	0.7261
				All data	0.3493	0.4576	0.5910	0.7530
BFGS		0.4145	−0.0015	Training	0.3382	0.4549	0.5815	0.7591
				Testing	0.3919	0.4970	0.6260	0.7261
				All data	0.3543	0.4675	0.5953	0.7494

Abbreviations: BFGS: Broyden–Fletcher–Goldfarb–Shanno; MAE: Mean absolute error; MSE: Mean squared error; RMSE: Root mean squared error; SAFER: Simple Algorithm For Evapotranspiration Retrieving.

A closer inspection of error metrics further supports these findings. In Scenario I, the testing RMSE and MAE were 0.5849 and 0.4548, respectively, while in Scenario II, they slightly decreased to 0.5696 and 0.4479, respectively. This reduction indicates improved prediction precision when additional training information is available. Importantly, the differences between training and testing errors remain relatively small in both scenarios, suggesting that the S/O–SAFER model does not exhibit significant overfitting and maintains strong generalization.

In contrast, the linear regression model showed consistently lower predictive performance across all evaluation metrics. Its testing R^2 values (0.7076 in Scenario I) are substantially lower than those of S/O–SAFER and are accompanied by higher error levels (RMSE = 0.6468). This behavior is primarily attributed to the model's inherent assumption of linearity, which limits its ability to capture nonlinear relationships in the dataset.

The optimization-based models, Nelder–Mead and BFGS, yielded intermediate performance. While they provided reasonable predictive accuracy, their results were less stable than those of S/O–SAFER. For instance, both Nelder–Mead and BFGS exhibit identical testing RMSE values (0.6260), indicating convergence to similar local solutions. However, their R^2 values (0.7261 for testing in both methods) remain significantly below those of the proposed model, reflecting limited modeling flexibility and sensitivity to optimization dynamics and initial conditions.

From a broader perspective, the comparison reveals that S/O–SAFER consistently achieved the best trade-off between accuracy and generalization across all scenarios. Unlike linear regression, which was constrained by linear assumptions, and Nelder–Mead/BFGS, which depended heavily on optimization behavior, S/O–SAFER maintained stable performance across training and testing partitions. This stability is particularly important for real-world applications where data variability and limited sample sizes are common challenges.

In summary, the results confirm that the proposed S/O–SAFER framework not only achieves higher predictive accuracy but also demonstrates superior robustness and generalization capability compared to conventional regression and optimization-based approaches.

4. Discussion

In a previous work, Karahan *et al.*[19] developed an ANN-based framework for estimating daily ETa by integrating satellite-observed days with long-term field measurements. Although that study demonstrated promising predictive capability, the ANN model was

trained on only approximately 5% of the available dataset, limiting its ability to fully exploit the information content of the observations. The authors noted that increasing the number of measurements could further improve model performance. In the present study, the same dataset was utilized to facilitate a direct comparison; however, the modeling philosophy differs substantially. Unlike the ANN approach, which is entirely data-driven, the proposed S/O–SAFER framework combines a physically based ETa formulation with a deterministic optimization strategy.

The results demonstrate that the proposed S/O–SAFER framework provides accurate and consistent ETa estimates under different calibration scenarios. Despite the substantial difference in training data size, both scenarios produced nearly identical optimal parameter values (Scenario I: $a = 0.3148$, $b = -0.0012$; Scenario II: $a = 0.3158$, $b = -0.0012$). This close agreement suggests that the optimization process converges toward a stable parameter region and that the calibrated SAFER formulation is relatively insensitive to the specific composition of the training dataset under the investigated conditions. The consistency of the optimized coefficients also indicates that the model structure effectively captures the dominant ETa dynamics across the study area.

A notable finding is that Scenario I, which relied exclusively on 38 satellite overpass days for calibration, achieved predictive performance comparable to that of Scenario II, which utilized a substantially larger training dataset. For the test dataset, Scenario I achieved $R^2 = 0.8195$ and RMSE = 0.5849, whereas Scenario II achieved $R^2 = 0.8249$ and RMSE = 0.5696. Across the entire dataset, the differences between the two scenarios remained negligible. These results indicate that reliable parameter calibration can be achieved using a limited number of observations, substantially reducing data requirements while maintaining predictive performance. From a practical perspective, this finding is particularly important for regions where long-term field measurements are unavailable or difficult to obtain.

Comparison with alternative calibration approaches further highlights the effectiveness of the proposed framework. Linear regression exhibited lower predictive accuracy, likely because the exponential structure of the SAFER equation cannot be adequately represented through a simple linear calibration procedure. Similarly, although Nelder–Mead and BFGS produced reasonable results, their performance was less consistent across datasets. In contrast, the SOS-based optimization framework yielded stable parameter estimates and maintained high predictive accuracy across both scenarios, indicating a better balance between exploration and exploitation during calibration.

Another important contribution of this study is the application of the SAFER model over a heterogeneous agricultural region characterized by multiple crop types and multiple growing seasons. Previous SAFER applications have generally focused on individual crops or relatively homogeneous agricultural environments. The presence of different crop species, varying phenological stages, and multiple harvest cycles introduces substantial spatial and temporal variability, making ETa estimation considerably more challenging. Nevertheless, the results demonstrate that the proposed framework can successfully capture ETa dynamics across diverse land-cover and cropping conditions without requiring crop-specific calibration.

Furthermore, compared with purely data-driven approaches such as ANNs, the proposed framework offers greater physical interpretability because the estimated ETa values remain directly linked to the underlying ETa formulation. This characteristic reduces dependence on large training datasets and provides a transparent calibration process while maintaining competitive predictive performance.

Overall, the strong agreement between observed and predicted ETa values, the consistency of the optimized coefficients across scenarios, and the robust performance achieved with limited calibration data demonstrate the reliability and practical applicability of the S/O–SAFER framework. In addition, the obtained results show generally good agreement with the simple methods proposed by Wang *et al.*[39] and Tegos *et al.*[40] These findings indicate that the proposed method is a robust and powerful tool for water resource management and operational ETa estimation, particularly in heterogeneous agricultural regions with limited data availability.

5. Conclusion

This study introduced a one-step S/O framework for calibrating the SAFER model and estimating daily ETa using remotely sensed variables and meteorological data. The proposed approach jointly optimizes the SAFER coefficients within a single optimization procedure, providing an alternative to conventional regression-based calibration methods.

The results demonstrated that both calibration scenarios produced highly similar parameter values and comparable predictive performance. Scenario I, which relied on only 38 satellite overpass days for calibration, achieved nearly the same accuracy as Scenario II, indicating that reliable ETa estimation can be obtained with substantially fewer data. The consistency of the optimized coefficients across scenarios further suggests a stable parameter region under the investigated conditions.

The successful application of the framework over a heterogeneous agricultural area containing multiple crop types and cropping cycles demonstrates its practical potential for large-scale ETa estimation. These findings indicate that the proposed S/O–SAFER framework constitutes a robust and efficient tool for supporting irrigation planning and water resource management, particularly in regions where extensive field measurements are unavailable.

It should be noted that the present study is based on a limited temporal dataset and does not cover a sufficiently long time period (e.g., multi-decadal records) to support a robust assessment of interannual variability or long-term persistence characteristics, such as those quantified by the Hurst exponent. Therefore, long-term clustering behavior of ETa could not be evaluated within the scope of this study. Future research incorporating longer time series would be valuable for further investigating these aspects.

Acknowledgments

None.

Funding

The dataset used in this study was obtained as part of the TÜBİTAK Project No. 122Y007, conducted under the supervision of the author. The author gratefully acknowledges TÜBİTAK for its financial support in acquiring these data.

Conflict of interest

The author declares no conflicts of interest.

Author contribution

This is a single-authored article.

Availability of data

Data are available on request from the author.

References

1. Bastiaanssen WGM, Menenti M, Feddes RA, Holtslag AAM. A remote sensing surface energy balance algorithm for land (SEBAL). 1. Formulation. *J Hydrol*. 1998;212-213:198-212.

   doi: 10.1016/s0022-1694(98)00253-4

2. Allen RG, Tasumi M, Trezza R. Satellite-Based Energy Balance for Mapping Evapotranspiration with Internalized Calibration (METRIC)—Model. *J Irrig Drain Eng*. 2007;133(4):380-394.

   doi: 10.1061/(asce)0733-9437(2007)133:4(380)

3. Senay GB, Bohms S, Singh RK, *et al*. Operational Evapotranspiration Mapping Using Remote Sensing and Weather Datasets: A New Parameterization for the SSEB Approach. *J Am Water Resour Assoc*. 2013;49(3):577-591.

   doi: 10.1111/jawr.12057

4. Teixeira AH de C. Determining Regional Actual Evapotranspiration of Irrigated Crops and Natural Vegetation in the São Francisco River Basin (Brazil) Using Remote Sensing and Penman-Monteith Equation. *Remote Sens*. 2010;2(5):1287-1319.

   doi: 10.3390/rs0251287

5. Roerink GJ, Su Z, Menenti M. S-SEBI: A simple remote sensing algorithm to estimate the surface energy balance. *Phys Chem Earth B*. 2000;25(2):147-157.

   doi: 10.1016/s1464-1909(99)00128-8

6. Santos JEO, Cunha FF da, Filgueiras R, *et al*. Performance of SAFER evapotranspiration using missing meteorological data. *Agric Water Manage*. 2020;233:106076.

   doi: 10.1016/j.agwat.2020.106076

7. Coaguila DN, Hernandez FBT, Teixeira AH de C, Franco RAM, Leivas JF. Water productivity using SAFER - Simple Algorithm for Evapotranspiration Retrieving in watershed. *Rev Bras Eng Agríc Ambient*. 2017;21(8):524-529.

   doi: 10.1590/1807-1929/agriambi.v21n8p524-529

8. Teixeira AH de C, Bastiaanssen WGM, Ahmad MD, Bos MG. Reviewing SEBAL input parameters for assessing evapotranspiration and water productivity for the Low-Middle São Francisco River basin, Brazil. *Agric For Meteorol*. 2009;149(3-4):462-476.

   doi: 10.1016/j.agrformet.2008.09.016

9. Teixeira AH de C, Takemura CM, Leivas JF, Pacheco EP, Bayma-Silva G, Garçon EAM. Water productivity monitoring by using geotechnological tools in contrasting social and environmental conditions: Applications in the São Francisco River basin, Brazil. *Remote Sens Appl Soc Environ*. 2020;18:100296.

   doi: 10.1016/j.rsase.2020.100296

10. Allen RG, Pereira LS, Raes D, Smith M. *Crop Evapotranspiration: Guidelines for Computing Crop Water Requirements*. Rome: Food and Agriculture Organization of the United Nations; 1998. (FAO Irrigation and Drainage Paper No. 56).

11. Hargreaves GH, Samani ZA. Reference Crop Evapotranspiration from Temperature. *Appl Eng Agric*. 1985;1(2):96-99.

    doi: 10.13031/2013.26773

12. Teixeira AH de C, Leivas JF, Hernandez FBT, Franco RAM. Large-scale radiation and energy balances with Landsat 8 images and agrometeorological data in the Brazilian semiarid region. *J Appl Remote Sens*. 2017;11(1):016030.

    doi: 10.1117/1.jrs.11.016030

13. Teixeira AH de C, de Miranda FR, Leivas JF, Pacheco EP, Garçon EAM. Water productivity assessments for dwarf coconut by using Landsat 8 images and agrometeorological data. *ISPRS J Photogramm Remote Sens*. 2019;155:150-158.

doi: 10.1016/j.isprsjprs.2019.07.006

14. Nadeem AA, Zha Y, Shi L, *et al*. SAFER-ET based assessment of irrigation patterns and impacts on groundwater use in the central Punjab, Pakistan. *Agric Water Manage*. 2023;289:108545.

doi: 10.1016/j.agwat.2023.108545

15. de Assis do Nascimento Leão F, Mercante E, Oliveira WKM, *et al*. Determination of evapotranspiration for citrus using SAFER algorithm in the Oriental Amazon. *Remote Sens Appl Soc Environ*. 2025;38:101526.

doi: 10.1016/j.rsase.2025.101526

16. Venancio LP, Mantovani EC, Amaral CH do, *et al*. Evapotranspiration mapping of commercial corn fields in Brazil using SAFER algorithm. *Sci Agric*. 2021;78(4).

doi: 10.1590/1678-992x-2019-0261

17. Souza JMF, Alves Jr J, Casaroli D, Evangelista AWP, Mesquita M. Validação do modelo SAFER na estimativa da evapotranspiração da cana-de-açúcar [Validation of the SAFER model for estimating sugarcane evapotranspiration]. *Irriga*. 2020;25(2):247-262.

doi: 10.15809/irriga.2020v25n2p247-262

18. Safre ALS, Nassar A, Torres-Rua A, *et al*. Performance of Sentinel-2 SAFER ET model for daily and seasonal estimation of grapevine water consumption. *Irrig Sci*. 2022;40(4-5):635-654.

doi: 10.1007/s00271-022-00810-1

19. Karahan H, Cetin M, Can ME, Alsenjar O. Developing a New ANN Model to Estimate Daily Actual Evapotranspiration Using Limited Climatic Data and Remote Sensing Techniques for Sustainable Water Management. *Sustainability*. 2024;16(6):2481.

doi: 10.3390/su16062481

20. Cetin M, Alsenjar O, Aksu H, Golpinar MS, Akgul MA. Comparing actual evapotranspiration estimations by METRIC to in-situ water balance measurements over an irrigated field in Turkey. *Hydrol Sci J*. 2023;68(8):1162-1183.

doi: 10.1080/02626667.2023.2198649

21. Cetin M, Karahan H, Golpinar MS, Alsenjar O, Can ME. Estimating actual evapotranspiration using the metric model and comparing it to in-situ hydrological measurements in an irrigated catchment. In: *5th International Conference on Research of Agricultural and Food Technologies (I-CRAFT 2025)*. Atlantis Press; 2026:153-163.

22. Tasumi M, Trezza R, Allen RG, Wright JL. Operational aspects of satellite-based energy balance models for irrigated crops in the semi-arid U.S. *Irrig Drain Syst*. 2005;19(3-4):355-376.

doi: 10.1007/s10795-005-8138-9

23. Didan K. MOD13Q1 MODIS/Terra Vegetation Indices 16-Day L3 Global 250m SIN Grid V006. NASA EOSDIS Land Processes DAAC; 2015.

doi: 10.5067/MODIS/MOD13Q1.006

24. Wan Z, Hook S, Hulley G. MODIS/Terra Land Surface Temperature/Emissivity Daily L3 Global 1 km SIN Grid V061. NASA EOSDIS Land Processes DAAC; 2021.

doi: 10.5067/MODIS/MOD11A1.061

25. Gorelick N, Hancher M, Dixon M, Ilyushchenko S, Thau D, Moore R. Google Earth Engine: Planetary-scale geospatial analysis for everyone. *Remote Sens Environ*. 2017;202:18-27.

doi: 10.1016/j.rse.2017.06.031

26. Dimitriadis P, Koutsoyiannis D, Iliopoulou T, Papanicolaou P. A global-scale investigation of stochastic similarities in marginal distribution and dependence structure of key hydrological-cycle processes. *Hydrology*. 2021;8(2):59.

27. Teixeira AH de C, Bastiaanssen WGM, Ahmad MD, Moura MSB, Bos MG. Analysis of energy fluxes and vegetation-atmosphere parameters in irrigated and natural ecosystems of semi-arid Brazil. *J Hydrol*. 2008;362(1-2):110-127.

doi: 10.1016/j.jhydrol.2008.08.011

28. de Queiroga Miranda R, Galvíncio JD, Moura MSB de, Jones CA, Srinivasan R. Reliability of MODIS Evapotranspiration Products for Heterogeneous Dry Forest: A Study Case of Caatinga. *Adv Meteorol*. 2017;2017:1-14.

doi: 10.1155/2017/9314801

29. Teixeira A, Leivas J, Takemura C, Garçon E, Sousa I, Azevedo A. Monitoring anomalies on large-scale energy and water balance components by coupling remote sensing parameters and gridded weather data. *Int J Biometeorol*. 2024;68(12):2597-2612.

doi: 10.1007/s00484-024-02771-w

30. Cheng MY, Prayogo D. Symbiotic Organisms Search: A new metaheuristic optimization algorithm. *Comput Struct*. 2014;139:98-112.

doi: 10.1016/j.compstruc.2014.03.007

31. Khalifeh S, Esmaili K, Khodashenas SR, Khalifeh V. Estimation of nonlinear parameters of the type 5 Muskingum model using SOS algorithm. *MethodsX*. 2020;7:101040.

doi: 10.1016/j.mex.2020.101040

32. Rezaei-Estakhroueiyeh A, Jalalkamali N, Momeniroghabadi M. Data on optimal operation of Safarud Reservoir using symbiotic organisms search (SOS) algorithm. *Data Brief*. 2020;29:105327.

doi: 10.1016/j.dib.2020.105327

33. Karahan H, Erkan Can M. A Novel Method to Forecast Nitrate Concentration Levels in Irrigation Areas for Sustainable Agriculture. *Agriculture*. 2025;15(2):161.

doi: 10.3390/agriculture15020161

34. Karahan H. Discussion of "Parameter Estimation of Nonlinear Muskingum Models Using Nelder-Mead Simplex Algorithm" by Reza Barati. *J Hydrol Eng*. 2013;18(3):365-367.

doi: 10.1061/(asce)he.1943-5584.0000667

35. Karahan H. Discussion of "Improved Nonlinear Muskingum Model with Variable Exponent Parameter" by Said M. Easa. *J Hydrol Eng*. 2014;19(10).

doi: 10.1061/(asce)he.1943-5584.0001045

36. Montgomery DC, Peck EA, Vining GG. *Introduction to Linear Regression Analysis*. 6th ed. John Wiley & Sons; 2021.

37. Nelder JA, Mead R. A Simplex Method for Function Minimization. *Comput. J*. 1965;7(4):308-313.

doi: 10.1093/comjnl/7.4.308

38. Nocedal J, Wright SJ. *Numerical Optimization*. 2nd ed. Springer; 2006.

39. Wang K, Wang P, Li Z, Cribb M, Sparrow M. A simple method to estimate actual evapotranspiration from a combination of net radiation, vegetation index, and temperature. *J Geophys. Res*. 2007;112(D15).

doi: 10.1029/2006jd008351

40. Tegos A, Malamos N, Koutsoyiannis D. A parsimonious regional parametric evapotranspiration model based on a simplification of the Penman–Monteith formula. *J Hydrol*. 2015;524:708-717.

doi: 10.1016/j.jhydrol.2015.03.024